ELSEVIER

Contents lists available at ScienceDirect

Earth and Planetary Science Letters

www.elsevier.com/locate/epsl



The quartz $\alpha \leftrightarrow \beta$ phase transition: Does it drive damage and reaction in continental crust?



Scott E. Johnson ^{a,*}, Won Joon Song ^a, Alden C. Cook ^b, Senthil S. Vel ^b, Christopher C. Gerbi ^a

- ^a School of Earth and Climate Sciences, University of Maine, Orono, ME 04469, USA
- ^b Department of Mechanical Engineering, University of Maine, Orono, ME 04469, USA

ARTICLE INFO

Article history: Received 27 April 2020 Received in revised form 24 September 2020 Accepted 30 September 2020 Available online xxxx Editor: R. Bendick

Keywords: quartz $\alpha \leftrightarrow \beta$ phase transition volumetric strain mechanical damage microcracking-enhanced fluid flow microcracking-enhanced reaction rheology

ABSTRACT

The $\alpha \leftrightarrow \beta$ phase transition in quartz is accompanied by relatively large, anisotropic changes in cell volume and elastic stiffness properties. Because quartz is among the most abundant minerals in Earth's continental crust, these changes have the potential to profoundly influence the state of stress, mechanical properties, metamorphism, and rheology of crustal rocks. Laboratory experiments confirm strongly enhanced microcracking as rocks cross the transition. In addition, limited seismological studies suggest that the $\alpha \leftrightarrow \beta$ transition may cause extensive microcracking in the crust. However, the micromechanical basis for potential transition-induced damage has not been quantitatively explored. Here we use numerical methods to show that elastic stresses arising from the transition can greatly exceed the brittle tensile and shear strengths of common crustal rocks and minerals at various confining pressures. In particular, we show that contraction during the down-temperature $\beta \to \alpha$ transition is far more effective than expansion during the up-temperature $\alpha \to \beta$ transition at promoting possible brittle failure and/or recrystallization (damage). Our results suggest that the $\alpha \leftrightarrow \beta$ transition may play an important role in damaging the continental crust, particularly in rock volumes that experience geologically rapid changes in temperature or pressure. In these environments, the transition may weaken rocks, establish transient permeability, facilitate advective mass transport and metamorphic reactions, and potentially nucleate earthquakes.

© 2020 Published by Elsevier B.V.

1. Introduction

Quartz is abundant in Earth's continental crust and is the only crustal mineral that undergoes a displacive phase transition under pressure and temperature conditions attainable under a variety of crustal conditions. At atmospheric pressure, the up-temperature $\alpha \to \beta$ transition for single-crystal quartz goes through an intermediate incommensurate phase at 573 °C and then to the β phase at 574.3 °C (Ohno et al., 2006). The transition temperature is pressure dependent (Fig. S1), with single-crystal transition temperatures increasing by approximately 0.255 °C/MPa (Shen et al., 1993). Limited studies of polyphase rocks show varied P-T relations for the transition in granitic type rocks (e.g., Kern, 1979; van der Molen, 1981), whereas P-T relations for the transition in a mica schist were effectively identical to those for single quartz crystals (Zappone and Benson, 2013). Although the transition involves a relatively minor rotation of the silica tetrahedra with respect to

* Corresponding author.

E-mail address: johnsons@maine.edu (S.E. Johnson).

one another, it is characterized by a volume change, with the β phase having the larger volume. The up-temperature $\alpha \to \beta$ transition for single crystals leads to volumetric expansion (2e $_1$ + e $_3$) of 6300 $\mu m/m$ (0.63%) and linear anisotropic extensional strains of e $_1$ = e $_2$ = 2400 $\mu m/m$ (0.24%) in the a-axis directions and e $_3$ = 1400 $\mu m/m$ (0.14%) in the c-axis direction (Carpenter et al., 1998).

In addition to the anisotropic volume change across the transition, there are large changes in the anisotropic elastic stiffness moduli. For example, Ohno et al. (2006) report values for all components of the elastic stiffness tensor either side of the transition boundary, at temperatures of 567 °C and 575.5 °C. Component values across this temperature range change sharply with, for example, C11 and C33 increasing from 69.2 and 67.4 GPa for the α phase at 567 °C, to 102.4 and 100.2 GPa for the β phase at 575.5 °C, respectively (Fig. S2a). The elastic properties of quartz at *both* elevated pressure and temperature are poorly understood (Abers and Hacker, 2017), and the Poisson's ratio of α -quartz is highly unusual compared to other silicates, becoming negative during the transition (Kern, 1979).

Owing to the 10–100 GPa-level values of the elastic stiffness moduli of common rock-forming minerals, we can expect such large changes in volume and stiffness to lead to large grain-scale stress concentrations relative to the typical brittle tensile and shear strengths of common crustal rocks and minerals. In addition, the anisotropic nature of these changes means that the crystallographic orientations of constituent quartz grains relative to one another and other minerals will lead to strong heterogeneity in the magnitudes and distributions of grain-scale stresses. Owing to the abundance of quartz throughout the continental crust and the progressive, sometimes abrupt, changes in confining pressure, temperature and differential stress with time in active tectonic settings, vast volumes of rock must cycle through the $\alpha \leftrightarrow \beta$ transition in both directions, possibly multiple times during their geological history.

Laboratory studies at atmospheric pressure have demonstrated that cycling quartz-bearing rocks across the transition temperature results in greatly increased microcracking above the background microcracking associated with thermal expansion. For example, acoustic emissions at atmospheric pressure show strong microcracking peaks across the up-temperature $\alpha \to \beta$ transition (Glover et al., 1995) and a reduced number of events when cycling back down temperature across the $\beta \rightarrow \alpha$ transition owing to extant up-temperature damage (Doncieux et al., 2008). Residual volume increase after thermal cycling indicates the development of significant microcrack porosity (Doncieux et al., 2008). In addition, large reductions in Young's modulus occur during three-point bending experiments in sandstone subjected to heating and cooling cycles through the $\alpha \leftrightarrow \beta$ transition, which is attributed to microcracking (Peng and Redfern, 2013). Indentation experiments (Lawn et al., 2020) also reported precipitous weakening of quartz near the $\alpha \leftrightarrow \beta$ transition by observing a marked drop in fracture strength at the transition. Experiments at confining pressures up to 300 MPa show evidence for microcracking related to thermal expansion during the up-temperature $\alpha \rightarrow \beta$ transition (e.g., Kern, 1979; van der Molen, 1981; Nikitin et al., 2009), but further experimental work is required to better define a confining pressure limit of microcracking associated with the transition.

Limited seismological studies suggest that the $\alpha \leftrightarrow \beta$ transition may cause widespread microcracking in the crust. For example, some workers (Marini and Manzella, 2005; Zappone and Benson, 2013) suggested that the $\alpha \leftrightarrow \beta$ transition is responsible for a high-amplitude seismic reflection (K-horizon) in the geothermal fields of Southern Tuscany, Italy. This horizon can be found at depths of \sim 3–9 km, appears to follow isotherms in the region, and is interpreted to represent fluid-bearing rocks that were strongly fractured during the $\alpha \leftrightarrow \beta$ transition. Others (e.g., Nikitin et al., 2009) have suggested that bursts of elastic acoustic emission oscillations during the $\alpha \leftrightarrow \beta$ transition demonstrate the discrete character of the instability and the possibility that such phenomena can contribute to the development of seismic events due to transition-related changes in the state of stress.

Owing to the rapid and large changes in stiffness between the α and β phases and the known pressure dependence of the transition for single-crystal quartz (Shen et al., 1993), seismologists have inferred the depth and temperature of the transition in several localities. Mechie et al. (2004) used the INDEPTH III seismic and electrical conductivity profiles in central Tibet to infer the quartz $\alpha \leftrightarrow \beta$ transition at a range of depths from \sim 13 to \sim 32 km. Kuo-Chen et al. (2012) used velocity ratios of P and S seismic waves to infer the quartz $\alpha \leftrightarrow \beta$ transition at \sim 24 km depth beneath Taiwan. Sheehan et al. (2014) used P and S velocity ratios to infer the quartz $\alpha \leftrightarrow \beta$ transition at \sim 50 km depth beneath southern Tibet.

Although the laboratory and seismological experiments noted above provide evidence for the role of the $\alpha \leftrightarrow \beta$ transition in damaging quartz-bearing rocks, there are no published studies that

calculate the grain-scale stress distributions and magnitudes in anisotropic polycrystalline rocks across a range of macroscale loading conditions and modal abundance of quartz. In addition, there are no experimental studies at elevated P and T explicitly designed to investigate damage caused by the down-temperature $\beta \to \alpha$ transition. These are necessary to validate conceptual mechanical models of damage resulting from the transition. Here we employ a novel numerical approach to calculate selected mechanical field variables for different loading conditions, using microstructures derived from electron backscatter diffraction (EBSD) data. We then discuss possible significance of the results.

2. Sample selection, EBSD data acquisition and post-processing

2.1. Sample selection

Two orthogneiss samples (MF223b and A18) and one quartz vein (NAP08-57) were chosen to examine the role of modal quartz abundance and microstructural heterogeneity on the range of grain-scale stress values (Fig. 1; Table S1). To investigate the role of modal quartz abundance, retaining the grain morphology of sample NAP08-57, we replaced the quartz crystallographic orientations with a distribution of random orientations and reassigned a percentage of the quartz grains to be plagioclase with random crystallographic orientations (Figs. 1 and S3). In doing this, synthetic samples with eleven modal quartz proportions from 0 to 100% were generated in 10% increments using the same randomized quartzplagioclase microstructure (Table S1). For each modal abundance, we made five different randomizations of quartz and plagioclase to show sample-scale heterogeneity related to spatial positioning and crystallographic orientation of each phase. The combination of three natural microstructures and the 55 randomly oriented microstructures with different quartz-plagioclase abundance allowed us to examine how the modal percentage of quartz and the presence of different phases affect the local stress distributions and magnitudes.

2.2. Data acquisition

The three natural samples were cut perpendicular to foliation and parallel to lineation, and polished mechanically with a 0.3 µm alumina suspension and chemically in a 0.02 µm colloidal silica suspension (for several minutes for mica-bearing samples and a couple of hours for the quartz vein). Electron backscatter diffraction (EBSD) maps were obtained on thin carbon coated samples to avoid electron charging, using the Tescan Vega II Scanning Electron Microscope equipped with an EDAX-TSL EBSD system at the University of Maine, USA. Simultaneous chemical analysis was performed via EDAX Genesis Energy Dispersive Spectroscopy. Diffraction patterns were acquired using EDAX-TSL OIM Data Collection 5.31 software at an acceleration voltage of 20 kV, a beam current of ${\sim}6$ nA, a 70° sample tilt, and high-vacuum conditions. EBSD data were collected with a square grid step size between 2 and 10 µm depending on average grain size and complexity in grain boundary shape. Raw indexing rates were >97%.

2.3. Post-processing

Post-processing of EBSD data involved first re-scanning the original maps using recorded Hough peaks and chemistry to accurately identify phases, improve indexing with optimized structure files, and eliminate minor phases (mostly opaque minerals <1%) for numerical analysis. Cleanup routines were conducted with EDAX-TSL OIM Analysis 5.31 software based on confidence index (CI) and neighboring phases and orientations. Pixels that could not be indexed or were poorly indexed (<minimum CI)

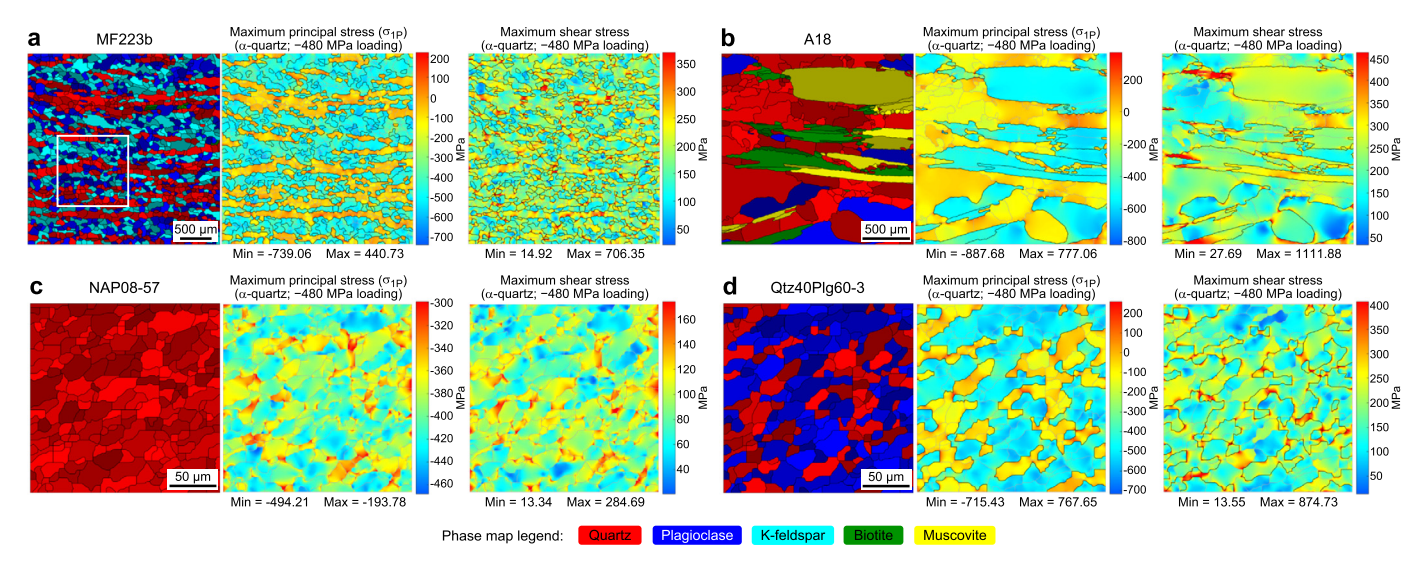


Fig. 1. Maximum principal stress (σ_{1P}) and maximum shear stress at hydrostatic loading in the presence of α-quartz. (a) MF223b – orthogneiss. (b) A18 – orthogneiss. (c) NAP08-57 – quartzite. (d) Qtz40Plg60-3 – an example of 'synthetic' rock with 40% randomized quartz and 60% randomized plagioclase using the same microstructure as (c). Left: combined phase and grain map. Center: maximum principle stress (σ_{1P}). Right: maximum shear stress. The phase maps with smoothed grain boundaries (as a result of meshing) were derived from the TESA Toolbox. Different shades of colors in the phase maps indicate different grains. See Fig. S3 for the phase maps and plotted crystallographic orientations measured by EBSD. Stresses in these samples were calculated for –480 MPa hydrostatic macroscale loading using α-quartz just below the transition at ~688 °C (Fig. S2d). (a), (b), and (d) show positive (tensile) values of σ_{1P} in quartz and negative values in other phases. (c) shows only negative (compressive) maximum principal stresses in the pure quartzite. A white box in (a) is the area of further numerical analysis for heterogeneous transition (see Section 4 and Fig. 5). (For interpretation of the colors in the figure, the reader is referred to the web version of this article.)

were replaced with well-indexed neighboring pixels of >minimum CI (0.1 for quartz vein; 0.02 for polyphase). The minimum CI of polyphase samples was determined by comparing photomicrographs and EBSD-derived maps of crystallographic orientation, phase and CI. The well-indexed pixels ranged between 67% and 85% of analyzed pixels. Since our numerical analysis using a finite element mesh requires perfectly bonded grain boundaries and single crystallographic orientation within a grain domain, any empty pixels (e.g., cracks or eliminated minor phases) were filled with neighboring phases, any twins (e.g., Dauphine twins in quartz or growth twins in feldspars) were removed, and all pixels making up a grain (with an internal misorientation <10°) were replaced by the average orientation for the grain. After automatic cleanup routines, partly mis-indexed mica and two feldspars were manually corrected using a pseudosymmetry cleanup routine, comparing EBSD maps and optical observation or photomicrographs (Fig. S3). Finally, for numerical analysis, the EBSD maps were cropped in a square shape, and Euler angles, pixel coordinates and phase information were exported.

3. Calculating grain-scale stresses: the homogeneous transition case

3.1. General approach

To investigate the grain-scale elastic stresses arising from the $\alpha \leftrightarrow \beta$ phase transition in quartz under different macroscale loading conditions, we employ the TESA (Thermo-Elastic and Seismic Analysis) numerical toolbox to apply the linear anisotropic transition strains (Appendix A). To model the up-temperature (or down-pressure) $\alpha \to \beta$ transition, we apply extensional strains of 2400 µm/m in the a-axis directions and 1400 µm/m in the c-axis direction to the quartz grains, each of which contains the stiffness tensor for β -quartz just above the atmospheric-pressure transition at 575.5 °C (Ohno et al., 2006). To model the down-temperature (or up-pressure) $\beta \to \alpha$ transition, we apply contractional strains of -2400 µm/m in the a-axis directions and -1400 µm/m in the c-axis direction to the quartz grains, each of which contains the

stiffness tensor for α -quartz just below the atmospheric-pressure transition at 567 °C (Ohno et al., 2006).

For the purposes of conducting numerical sensitivity analyses, all samples were placed under hydrostatic (isotropic) macroscale loading of -130, -270 and -480 MPa (noting that compression is negative) corresponding roughly to depths of 5, 10 and 18 km, respectively. The smaller two hydrostatic loading conditions (-130 and -270 MPa) would apply to areas of high heat flow, such as the geothermal fields in Southern Tuscany showing the K-horizon (e.g., Marini and Manzella, 2005). The larger loading condition (-480 MPa) would loosely apply to areas where the $\alpha \leftrightarrow \beta$ transition has been inferred from seismological observations at deeper crustal depths ranging from \sim 15 to 50 km (Mechie et al., 2004; Kuo-Chen et al., 2012; Sheehan et al., 2014).

3.2. Projecting atmospheric-pressure stiffness data to higher pressures

The numerical calculations were made at temperatures of 567 °C and 575.5 °C, either side of the $\alpha \leftrightarrow \beta$ transition, using the 1 atm stiffness tensors from Ohno et al. (2006). The only experimentally determined stiffness tensors that cross the phase transition are those conducted at atmospheric pressure across a range of temperatures (Ohno et al., 2006; Lakshtanov et al., 2007). Experiments conducted at room temperature across a range of pressures cannot cross the phase transition into the β stability field so are not relevant to the present study. Owing to the lack of experimental data varying both temperature and pressure, it is common practice in geophysics and petrophysics to use quartz stiffness tensors determined at atmospheric pressure to, for example, (a) calculate/interpret seismic wave speeds throughout the crust and (b) infer geothermal gradients by using ratios of P- and S-wave velocities to determine the depth of the $\alpha \leftrightarrow \beta$ transition (Mechie et al., 2004; Kuo-Chen et al., 2012; Sheehan et al., 2014; Abers and Hacker, 2017).

Because we are using stiffness tensors determined at atmospheric pressure, the temperature axis in the graph of quartz stiffness moduli versus temperature needs to be "shifted" before we can evaluate the transition at the elevated macroscale pressure of interest. We used the results of Shen et al. (1993) to shift the tem-

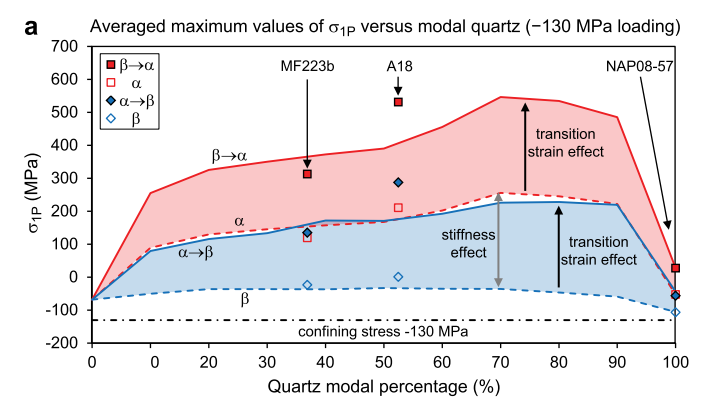
perature axis for macroscale confining pressures of -130, -270 and -480 MPa (Table S2; Fig. S2). In shifting the temperature axis, we assume that a complete data set of stiffnesses at both elevated temperature and pressure would probably change the absolute values of calculated stresses but would not alter our fundamental conclusions from the numerical results presented in the following sections.

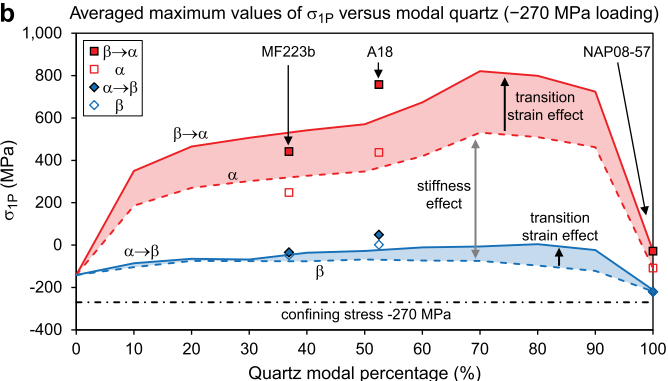
3.3. Numerical results

It is instructive to first calculate the total elastic stresses that would accumulate if all quartz grains changed their phase simultaneously. This homogeneous transition model explicitly allows: (a) quantitative assessment of the role of modal mineralogy in local stress magnitudes and distributions, (b) comparison of stresses related to the change in elastic stiffness tensor with those related to the phase-transition strains, and (c) evaluation of how their relative contributions change with confining pressure.

Inelastic deformation of rocks in Earth's continental crust is commonly described in terms of tensile and/or shear stress criteria, so we chose two quantities to compare across the range of samples to illustrate the effect of microstructure and quartz mode: (1) maximum principal stress σ_{1P} noting that tension is positive; and (2) maximum shear stress $1/2(\sigma_{1P} - \sigma_{3P})$. Fig. 1 shows mineral phase maps and examples of these two quantities for the different microstructures, and Fig. S3 displays their photomicrographs and EBSD phase maps with associated crystallographic preferred orientations. Fig. 2 compares averaged maximum values of σ_{1P} for the five synthetic samples for each quartz mode between α -quartz just below the transition with no applied transition strains, β -quartz just above the transition with no applied transition strains, and the same α - and β -quartz with applied strains associated with the $\alpha \to \beta$ and $\beta \to \alpha$ transitions. The maximum value of σ_{1P} of the three natural samples is also plotted in Fig. 2. The maximum, minimum and average values of σ_{1P} and $1/2 \, (\sigma_{1P} - \sigma_{3P})$ for all samples and simulations are shown in Fig. S4 and Data S1. The first-order observations are as follows.

- Although the samples were placed under compressive macroscale loads, large tensile principal stresses (positive σ_{1P}) and shear stresses arise during the down-temperature $\beta \rightarrow \alpha$ transition (Figs. 2 and S4), both as a function of changes in elastic stiffness tensor and the linear transformation strains (Fig. 2). Excluding the transformation strains, the change in stiffness tensor from $\beta \to \alpha$ leads to maximum positive changes in σ_{1P} of 292 MPa, 607 MPa and 1079 MPa for macroscopic loads of -130, -270 and -480 MPa, respectively ('stiffness effect' in Fig. 2). The transition strains add a maximum positive change in σ_{1P} of \sim 290 MPa for each of the three macroscale loads ('transition strain effect' in Fig. 2). Although not shown, proportionally similar changes occur for shear stress. We note that the 100% quartz rock does not accumulate large stresses upon complete transition (Figs. 2 and S4) because the entire rock simply undergoes a macroscale volumetric contraction.
- Adding plagioclase to quartz in the randomized samples increases elastic inhomogeneity, which increases the range in stress values (Figs. 1, 2 and S4). This increased range is driven by the elastic mismatches and strong anisotropies of the two phases.
- Values of both quantities for the natural microstructures lie near values of the randomized quartz-plagioclase microstructures, for equivalent quartz abundance (Figs. 2 and S4), the variation largely due to additional phases and non-random crystallographic orientations.
- The greater compliance and anisotropy of α-quartz relative to β-quartz leads to greater elastic mismatch with plagioclase, as





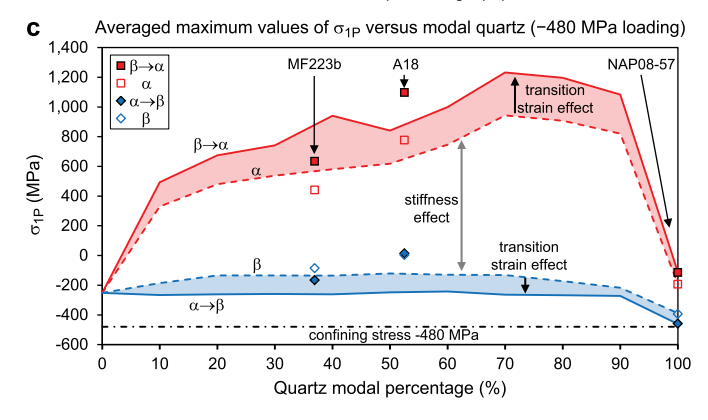


Fig. 2. Averaged maximum values of the maximum principal stress (σ_{1P}) versus quartz modal abundance for α , β , $\alpha \to \beta$, and $\beta \to \alpha$. The curves are averages of the five samples for each quartz mode shown in Fig. S4. The four curves show α -quartz (red dashed curve), β -quartz (blue dashed curve), quartz that experienced the $\alpha \to \beta$ transition (blue solid curve), and quartz that experienced the $\beta \to \alpha$ transition (red solid curve). The data are for hydrostatic macroscale loads of (a) -130 MPa, (b) -270 MPa, and (c) -480 MPa, respectively. These diagrams illustrate the varying contributions of changes in the stiffness tensor (α versus β) and the transition strains with increasing confining pressure. The contributions from change in elastic stiffness are shown as gray arrows ('stiffness effect'), and the linear transition strains are shown as black arrows ('transition strain effect') with color shades. Note the strongly increasing contribution of the changing stiffness tensor with increasing confining pressure. (For interpretation of the colors in the figure, the reader is referred to the web version of this article.)

shown by the spread of maximum values of both variables in Fig. S4.

4. Calculating grain-scale stresses: the heterogeneous transition case

It is apparent in the homogeneous transition case (Figs. 2 and S4) that peak elastic stress values associated with the $\alpha \leftrightarrow \beta$ transition, and particularly the $\beta \rightarrow \alpha$ transition, greatly exceed the brittle strength of rocks at many numerical quadrature points

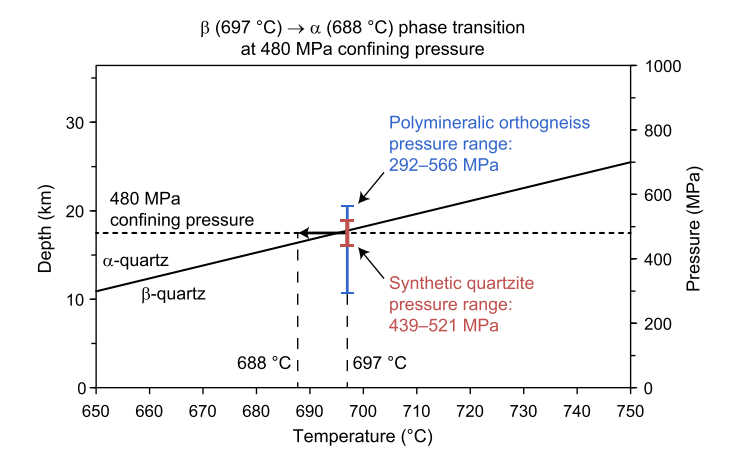


Fig. 3. Description of the $\beta \to \alpha$ phase transition of a synthetic quartzite and a polymineralic orthogneiss at 480 MPa confining pressure. The vertical red and blue bars indicate the ranges of quartz grain-scale pressure (absolute value of TESA mean stress only in quartz) calculated for 480 MPa confining pressure in the quartzite and orthogneiss, respectively, using β -quartz just above the transition at \sim 697 °C (Fig. S2d). During cooling to \sim 688 °C, β -quartz grains that reach the phase transition boundary are transformed to α -quartz. The pressure ranges are expected to rapidly decrease as the transition progresses owing to the "focusing" effect proposed by Coe and Paterson (1969). (For interpretation of the colors in the figure, the reader is referred to the web version of this article.)

in the microstructure. However, those solutions represent the endmember case in which we calculate the total elastic stress associated with complete phase transition. In nature, the grain-scale stresses would never reach the large values shown in the homogeneous transition results because rapidly accumulating elastic stresses would be dissipated by inelastic processes such as microcracking and viscous flow until the rock is no longer at a critical state. To demonstrate this self-limiting feedback, we explore the stresses arising from progressive single-grain transitions in both a monomineralic synthetic quartzite (a randomized sample using the grain morphology of sample NAP08-57) and a polymineralic orthogneiss consisting of quartz, plagioclase and K-feldspar (a subarea of sample MF223b; white box in Fig. 1a) and illustrate the inelastic dissipation of these stresses by microcracking using a tensile failure criterion (see Appendix A).

For the heterogeneous transition case, we consider first the randomized quartzite on a -480 MPa isobaric cooling path passing through the β field across the $\beta \to \alpha$ transition (Fig. 3). Showing this scenario in P–T space along with the total range of grainscale pressure calculated for -480 MPa confining pressure in the quartzite using β -quartz just above the transition at \sim 697 °C, the pressure range in the β -quartz grains straddles the phase transition at that temperature (Fig. 3). Thus, the grains with the highest local pressures would begin transitioning to α -quartz grains, and pressures would then be redistributed to other β -quartz grains pushing them over the transition (see Section 5.2 for a discussion).

To simulate the accumulation and dissipation of excess elastic stresses, we begin by assigning all grains the stiffness tensor of β -quartz at \sim 697 °C (Fig. S2d) and a tensile strength of 50 MPa, and apply hydrostatic macroscale loading of -480 MPa. Macroscopic tensile strength of some quartzites has been shown experimentally to be \sim 10 MPa (Mardon et al., 1990), and Lawn et al. (2020) showed using indentation experiments that the fracture strength of Z-cut single quartz crystals drops to nearly zero at the transition; thus, our choice of 50 MPa is very conservative in that a lower tensile strength would result in more microcracking. As expected (β -quartz in Fig. 2c), none of the β -quartz grains show tensile principal stresses. We then search the microstructure for the β -quartz grain with the most negative mean stress (highest pressure) and change that grain to α -quartz using the stiffness ten-

sor of α -quartz at \sim 688 °C (Fig. S2d). We transform one grain with the highest pressure and let the simulation run until σ_{1P} in all elements drops below the 50 MPa tensile strength threshold. Repeating this exercise for 200 numerical steps, transforming one grain at a time, leads to seven transformed grains and six cycles of tensile stress exceeding the failure criterion followed by microcracking and dissipation of the elastic stresses (Fig. 4; Animation S1). Microcracks tend to form preferentially along the quartz-quartz grain boundaries, to a lesser degree migrating within and across grains (Fig. 4; Animation S1). The preference for grain-boundary microcracking results from stress concentrations caused by a combination of elastic mismatches at grain contacts and elastic anisotropy of individual grains, particularly directly after the contraction caused by grain transition.

Second, we consider the polymineralic orthogneiss, also on a 480 MPa isobaric cooling path passing through the β field across the $\alpha \leftrightarrow \beta$ phase transition boundary (Fig. 3). Using β -quartz just above the transition at \sim 697 °C, the pressure range in the β -quartz grains straddles the phase transition at that temperature, much like the quartzite discussed above, though the pressure range in the quartz grains is larger owing to the polyphase nature of the rock (Fig. 3). The grains with the highest local pressures would begin transitioning to α -quartz grains, and pressures would then be redistributed to other β -quartz grains thus pushing them over the transition. As with the quartzite, we transform one quartz grain with the highest pressure and let the simulation run until the maximum principal stress in all elements drops below the 50 MPa tensile strength threshold. Repeating this exercise for 1000 numerical steps, transforming one grain at a time, leads to only three transformed grains (Fig. 5; Animation S2). After the third grain transforms, the maximum principal stress never drops below the 50 MPa tensile strength threshold, and the microstructure undergoes continued failure owing to (a) the role of elevated local stress heterogeneities caused by multiple anisotropic phases and (b) the tensile stresses caused by the reduction in strength of damaged elements.

Microcracks in the polyphase sample also tend to prefer the boundaries of newly transformed quartz grains similar to the quartzite simulation, but continued microcracking in the feldspars shows no obvious preference for grain boundaries (Fig. 5 and Animation S2), suggesting that the sudden contraction associated with quartz transition is the primary driver for the grain-boundary preference. For the purposes of this paper, grain boundaries were assigned the same strength as grains. Weakening boundaries relative to grains would lead to more focused microcracking along the boundaries.

5. Discussion

5.1. Dissipation processes and thermodynamic considerations

Owing to changes in confining pressure, temperature and tectonic stress with time in active tectonic settings, vast volumes of crustal rock will cycle through the $\alpha \leftrightarrow \beta$ transition in response to thermal and stress perturbations caused, for example, by episodic partial melting, melt migration, magma-chamber formation and seismicity with associated fluid advection. These and other processes can lead to geologically rapid changes in temperature and stress state over significant rock volumes. If we assume that individual grains undergo effectively instantaneous transition, brittle response to the large local tensile stresses would be extremely rapid with tensile crack propagation velocities limited by the Rayleigh speed. Because fracture is a relatively weak energy dissipation process (Sharon et al., 1996), extensive microcracking should be expected where the initial response is brittle. Once the

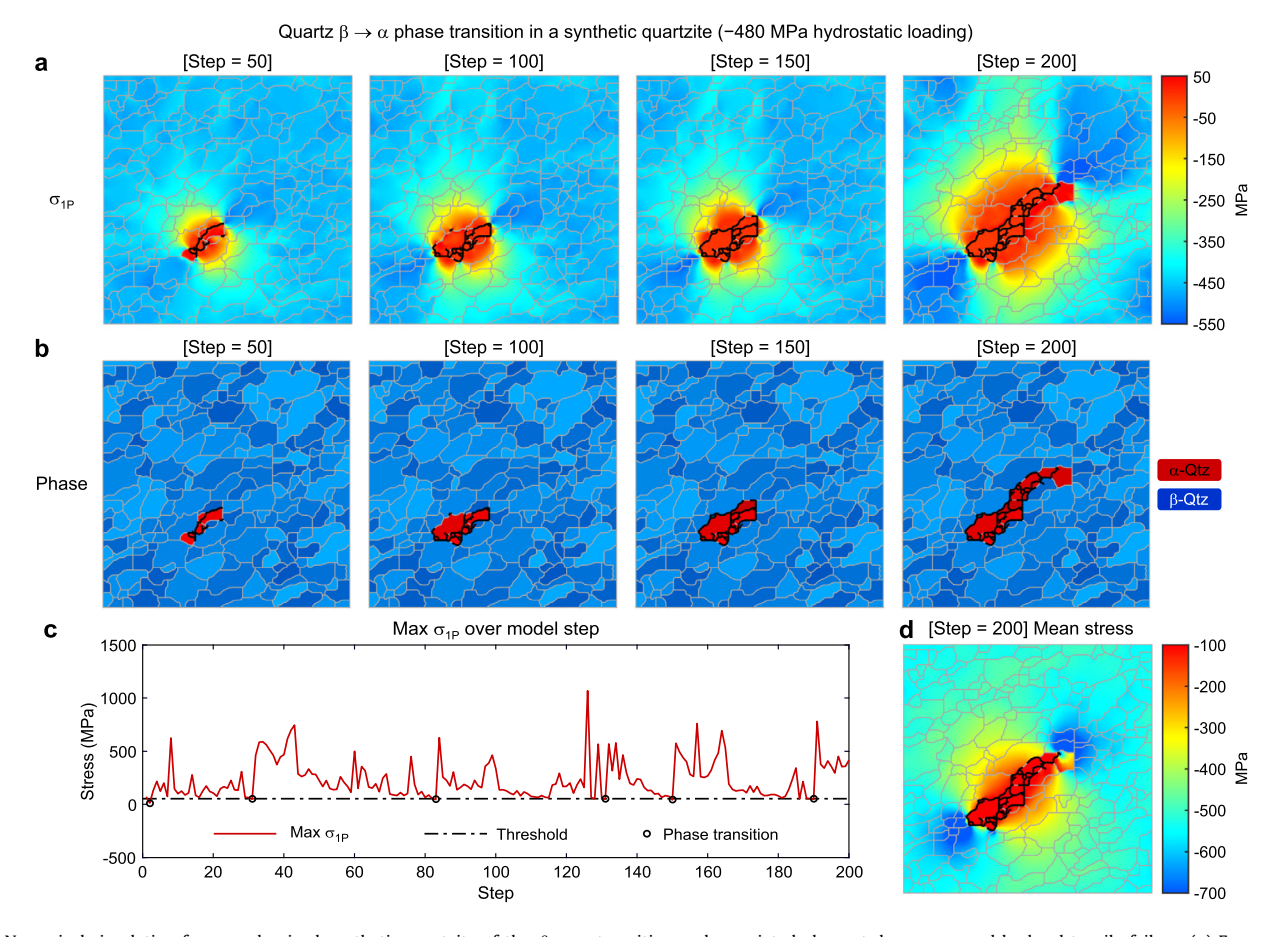


Fig. 4. Numerical simulation for a randomized synthetic quartzite of the $\beta \to \alpha$ transition and associated element damage caused by local tensile failure. (a) Four snapshots of maximum principal stress (σ_{1P}) map at model steps of 50, 100, 150 and 200. (b) Four snapshots of phase map β -quartz (β -Qtz) in blue and α -quartz (α -Qtz) in red at model steps of 50, 100, 150 and 200. Different shades of blue and red indicate different grains or crystallographic orientations. (c) Evolution of the maximum element value of σ_{1P} over 200 numerical steps. (d) A snapshot of mean stress map at model step of 200. All grains begin as β -quartz with a tensile strength of 50 MPa under hydrostatic macroscale loading of -480 MPa. β grains with the most negative mean stress are changed to α grains, one at a time, when the maximum principal stress drops below the 50 MPa tensile strength threshold. The thick black lines in (a), (b) and (d) indicate damaged elements that once had σ_{1P} above the tensile strength threshold (see Appendix A). See Animation S1 for evolution through all 200 steps. (For interpretation of the colors in the figure, the reader is referred to the web version of this article.)

tensile stresses drop below the cracking threshold, viscous flow could further dissipate some of the remaining stress peaks.

The transition is accompanied by the formation of Dauphiné twins (Wenk et al., 2009) which would increase stored elastic stress. In addition, quartz has a very low viscosity at transition temperatures, and the transition may be accompanied by sharply reduced creep strength in quartz (Schmidt et al., 2003; Lawn et al., 2020). Thus, rocks near the transition may be particularly susceptible to quartz grain size reduction through viscous flow and recrystallization. Assuming an appropriate differential stress, reduced creep strength in quartz at the transition combined with Dauphiné twinning and grain size reduction may be a critical factor in viscous strain localization. It is worth noting in this context that grain-scale elastic stresses cannot be fully dissipated by viscous processes because they arise from the interactions of the individual elastically anisotropic grains. Rocks under confining pressure will always harbor elastic stresses arising from elastic strains plus grain interactions. Brittle or viscous microstructural adjustments can reduce the magnitudes of local stress peaks but cannot eliminate/dissipate local elastic stresses as might be envisaged for a simple visco-elastic material. Such residual stresses represent significant stored energy that is available for other processes such as dissolution-precipitation creep and metamorphic reactions.

Strong changes in thermodynamic quantities also occur across the transition and it is worth considering their potential impact. Temperature change ΔT can be inferred from the change in enthalpy ΔH and the heat capacity Cp as ΔH = Cp \times ΔT . Using

data from Ghiorso et al. (1979) and Carpenter et al. (1998), ΔH for the $\beta \to \alpha$ transition ranges from approximately -400 to -800 J/mol, making the transition exothermic. Considering Cp values for the α phase, there is a steep increase near the transition temperature where Cp is greater than 90 J/(mol × °K) (e.g., Carpenter et al., 1998). Thus, an upper bound on the change in temperature $\Delta T = \Delta H$ / Cp is approximately -4.4 to -8.9 °C. This negative temperature change would tend to stabilize grains that experience the $\beta \to \alpha$ transition. Release of latent heat into the surroundings may delay the onset of transition for surrounding β -grains, though the focusing effect described in Section 5.2 may well dominate over this thermal effect.

Regardless of the mechanism for dissipating the excess elastic stress arising from the $\alpha\leftrightarrow\beta$ transition, the transition can be viewed as an irregular damage horizon passing through regions of continental crust where the geothermal gradient is high enough and/or local stress/temperature perturbations occur. Thus, it might occur at depths of less than 5 km in geothermal fields where thermal gradients can reach >120 °C/km (Fig. 2a; e.g., Marini and Manzella, 2005), or at greater depths in active convergent tectonic settings (Fig. 2c; e.g., Mechie et al., 2004; Kuo-Chen et al., 2012; Sheehan et al., 2014).

5.2. Rate of $\alpha \leftrightarrow \beta$ transition in polycrystalline rocks

Because the $\alpha \leftrightarrow \beta$ transition in polycrystalline rocks is dependent on hydrostatic pressure (e.g., Kern, 1979; van der Molen,

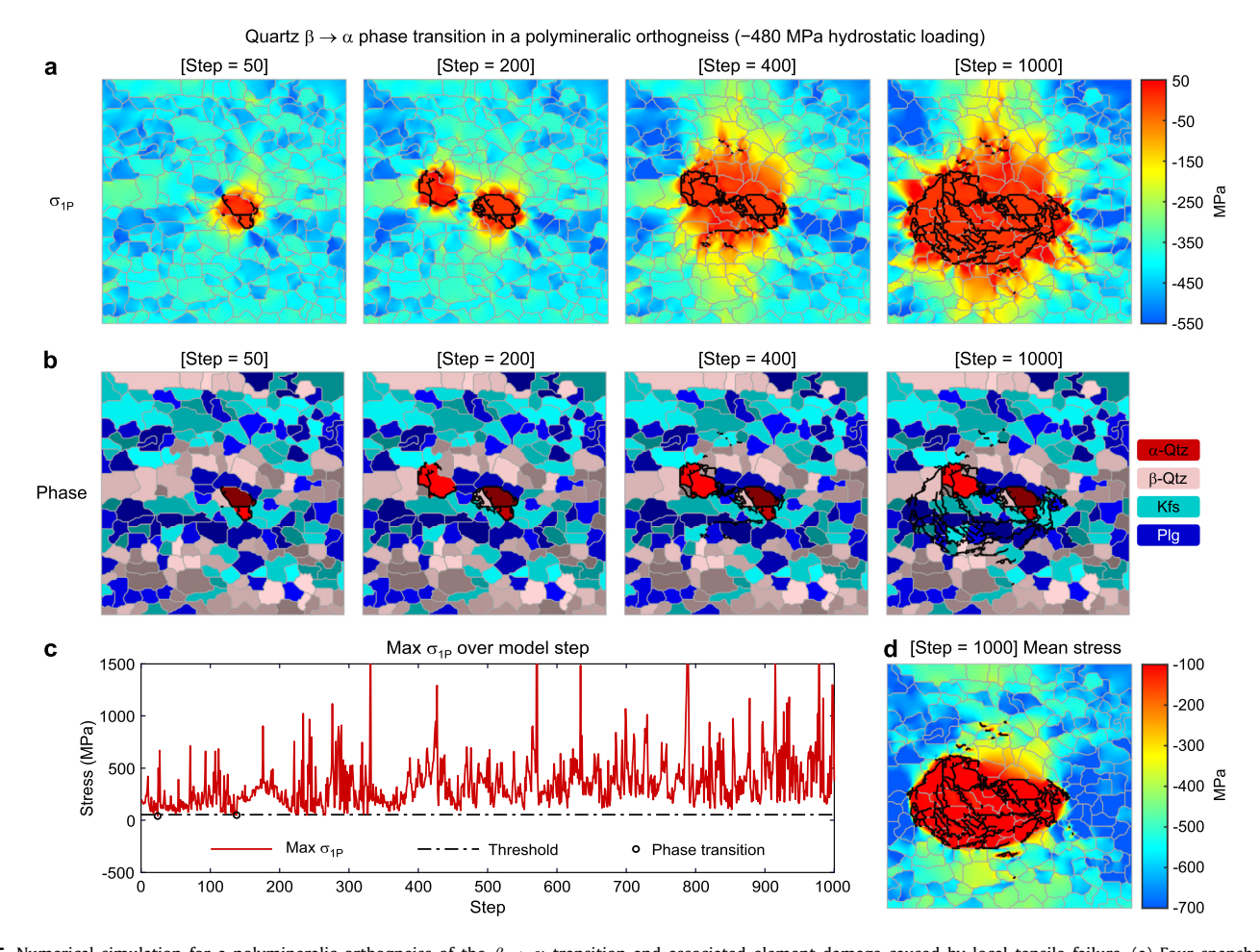


Fig. 5. Numerical simulation for a polymineralic orthogneiss of the $\beta \to \alpha$ transition and associated element damage caused by local tensile failure. (a) Four snapshots of maximum principal stress (σ_{1P}) map at model steps of 50, 200, 400 and 1000. (b) Four snapshots of phase map β -quartz (β -Qtz) in pink, α -quartz (α -Qtz) in red, K-feldspar (Kfs) in cyan and plagioclase (Plg) in blue at model steps of 50, 200, 400 and 1000. Different shades of the colors indicate different grains or crystallographic orientations. (c) Evolution of the maximum element value of σ_{1P} over 1000 numerical steps. (d) A snapshot of mean stress map at model step of 1000. All grains have a tensile strength of 50 MPa under hydrostatic macroscale loading of -480 MPa, and all quartz grains begin as β -quartz. β grains with the most negative mean stress are changed to α grains, one at a time, when the maximum principal stress drops below the 50 MPa tensile strength threshold. The thick black lines in (a), (b) and (d) indicate damaged elements that once had σ_{1P} above the tensile strength threshold (see Appendix A). See Animation S2 for evolution through all 1000 steps. (For interpretation of the colors in the figure, the reader is referred to the web version of this article.)

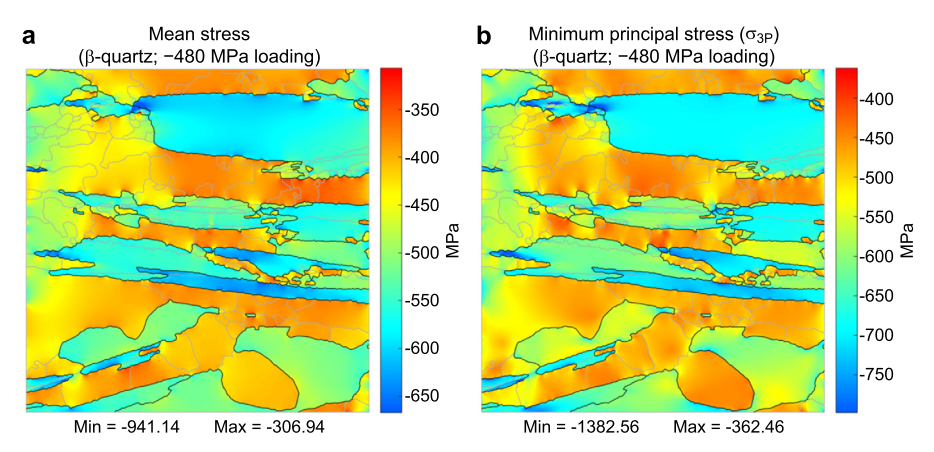


Fig. 6. Grain-scale variations of stresses for sample A18. (a) Map of mean stress distribution. (b) Map of minimum principal stress (maximum compressive stress) distribution. See Fig. 1b for the phase map. Stresses were calculated for -480 MPa hydrostatic macroscale loading using β-quartz just above the transition at \sim 697°C (Fig. S2d). Note high heterogeneous stress distributions with a range of several hundred MPa in β-quartz. (For interpretation of the colors in the figure, the reader is referred to the web version of this article.)

1981; Shen et al., 1993; Fig. S1) and, to a lesser extent, crystal-lographic orientation relative to the local principal stresses under nonhydrostatic loading (Coe and Paterson, 1969), individual quartz grains in a rock might be expected to transform at different times

over a substantial range of macroscale pressure and temperature conditions; however, there are reasons to doubt this. Fig. 6a shows grain-scale mean stress or pressure $(1/3 [\sigma_{11} + \sigma_{22} + \sigma_{33}])$ distributions for hydrostatic loading of -480 MPa with β -quartz at

 \sim 697 °C (Fig. S2d). Pressure distribution in the β -quartz is highly heterogeneous and spans a range of several hundred MPa. As the $\beta \to \alpha$ transition temperature for the macroscale pressure is approached during isobaric cooling, grains with the highest local pressure and favorable crystallographic orientation would be first to transition to the higher density α phase. Transition of these first grains would be accompanied by a volume reduction and precipitous drop in their bulk modulus (e.g., Ohno et al., 2006; Lakshtanov et al., 2007), and the resulting elastic softening would redistribute the higher pressures to other β -quartz grains that would in turn undergo the transition.

This redistribution and homogenization of pressures is the "focusing" effect proposed by Coe and Paterson (1969) and van der Molen (1981), which is likely to cause the transition for all grains to occur rapidly over a narrow temperature/pressure window. Recent work (Richter et al., 2016) indicates that the phase transition from α -quartz to coesite under nonhydrostatic stress is more directly dependent on the macroscale maximum compression than it is on mean stress. Fig. 6b shows a map of minimum principal stress (maximum elastic compressive stress). As expected, its distribution in the β -quartz is highly heterogeneous and spans a range of several hundred MPa. The grain-scale stress distributions in Fig. 6 show information that cannot be directly obtained in laboratory experiments where results must be interpreted based on the macroscale loading, although in-situ measurements of lattice spacing using neutron diffraction has shown that grain-scale stresses significantly exceed macroscale stresses by up to a factor of three or four (e.g., Nikitin et al., 2006).

5.3. Transition stress, seismicity, permeability, and metamorphic reactions

The highly heterogeneous mean and principal normal stresses in anisotropic polycrystalline rocks (Fig. 6) and large tensile stresses generated during the $\beta \to \alpha$ transition (Figs. 4 and 5; Animations S1 and S2), may have important implications for seismicity, the development of transient permeability, and progress of metamorphic reactions.

5.3.1. Seismicity and seismic observations supporting transition-induced damage

A causal relationship between seismicity and the transition was proposed by Marini and Manzella (2005) and Zappone and Benson (2013) in the hydrothermal fields of Southern Tuscany, where high-amplitude seismic anomalies (the K-horizon) thought to arise from fluid-filled microcracks can be found at depths of $\sim\!3-9$ km. Using thousands of seismic events, Marini and Manzella (2005) showed that the depth of the K-horizon roughly coincides with the depths of hypocenter occurrences. The relatively high temperature ($\sim\!600-650\,^\circ\text{C}$) of the transition at these depths would place the rocks spatially well below the typical upper-crustal seismicity cutoff depth, lending support to their proposal that the $\alpha\leftrightarrow\beta$ transition may be a contributing cause of the seismicity.

Sheehan et al. (2014) identified a region of high longitudinal- and shear-wave attenuation (low Q_P and Q_S) at 45–50 km depth under the Tibetan plateau that corresponds to the location of the $\alpha \leftrightarrow \beta$ transition as determined by the ratio of compression-to shear-wave velocities (V_P/V_S) . Based on these and other data, they suggested that the region of high attenuation may be due to trapped aqueous fluid in felsic crustal rocks at the quartz $\alpha \leftrightarrow \beta$ transition. One implication is that the fluid may be hosted in microcracks generated by the $\alpha \leftrightarrow \beta$ transition.

Nikitin et al. (2009) stated that the buildup of grain-scale elastic stresses during the $\alpha \leftrightarrow \beta$ transition can reach values close to a rock's tensile strength, causing loss of the rock's mechanical stability. In fact, our results for the $\beta \to \alpha$ transition, which have

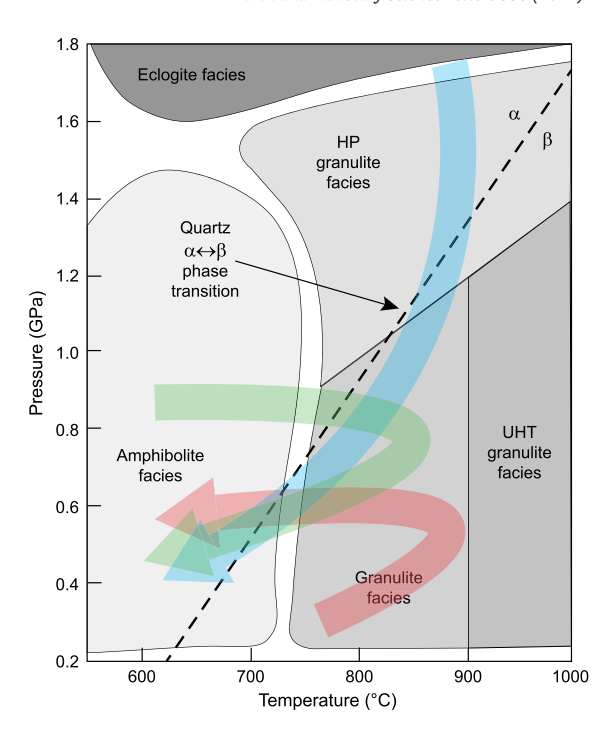


Fig. 7. Diagram showing three generalized paths (color shaded arrows) in pressure-temperature space for rocks that cross the $\alpha \leftrightarrow \beta$ transition from granulite- to amphibolite-facies metamorphic conditions. Metamorphic facies are after Brown (2007) and Vernon and Clarke (2008). Generalized representative paths are after Spear (1992), Zhang et al. (2015) and Blereau et al. (2017). HP = high-pressure; UHT = ultrahigh-temperature. (For interpretation of the colors in the figure, the reader is referred to the web version of this article.)

apparently been difficult to explore experimentally without preexisting damage bias from the $\alpha \to \beta$ transition, show that tensile stresses can be much larger than the tensile strength. It might be a fruitful future direction to conduct experiments aimed explicitly at the $\beta \to \alpha$ transition.

5.3.2. Transient permeability and metamorphic reactions

Metamorphism facilitates geodynamically important changes in the continental crust, modulating density, heat production and rheology. It is increasingly apparent that dry amphibolite- and granulite-facies metamorphic rocks in the middle and lower continental crust are typically not in chemical equilibrium and would rapidly react if exposed to fluids (Jamtveit et al., 2016). Introducing fluids to dry rock is readily accomplished through microcrackgenerated permeability or viscous strain localization that involves grain-scale dilatation. Although metamorphic reactions themselves can be responsible for relatively large volume changes and resulting stresses capable of cracking rocks, brittle damage during seismicity (Jamtveit et al., 2019) and/or the $\alpha \leftrightarrow \beta$ transition can facilitate fluid access required to initiate reaction progress. Pressuretemperature-time paths in granulite-facies rocks commonly cross the $\beta \to \alpha$ transition on a retrograde metamorphic path near the transition temperature from granulite to amphibolite facies metamorphism of \sim 650–750 °C (Fig. 7).

As quartz-bearing granulite-facies rocks pass through the $\beta \to \alpha$ transition, they may undergo extensive microcracking, allowing infiltration of any available fluids and the initiation of hydrated amphibolite-facies shear zones overprinting the granulite-facies rocks. It might be expected that brittle crack opening would be suppressed at these higher pressures, but there are many examples of fluid-inclusion-bearing healed microcracks that formed near the $\beta \to \alpha$ transition in granulite-facies rocks. Fig. 8 shows a collection of healed microcracks, some lined with fluid inclusions, which formed in a granulite-facies rock at about the time that it

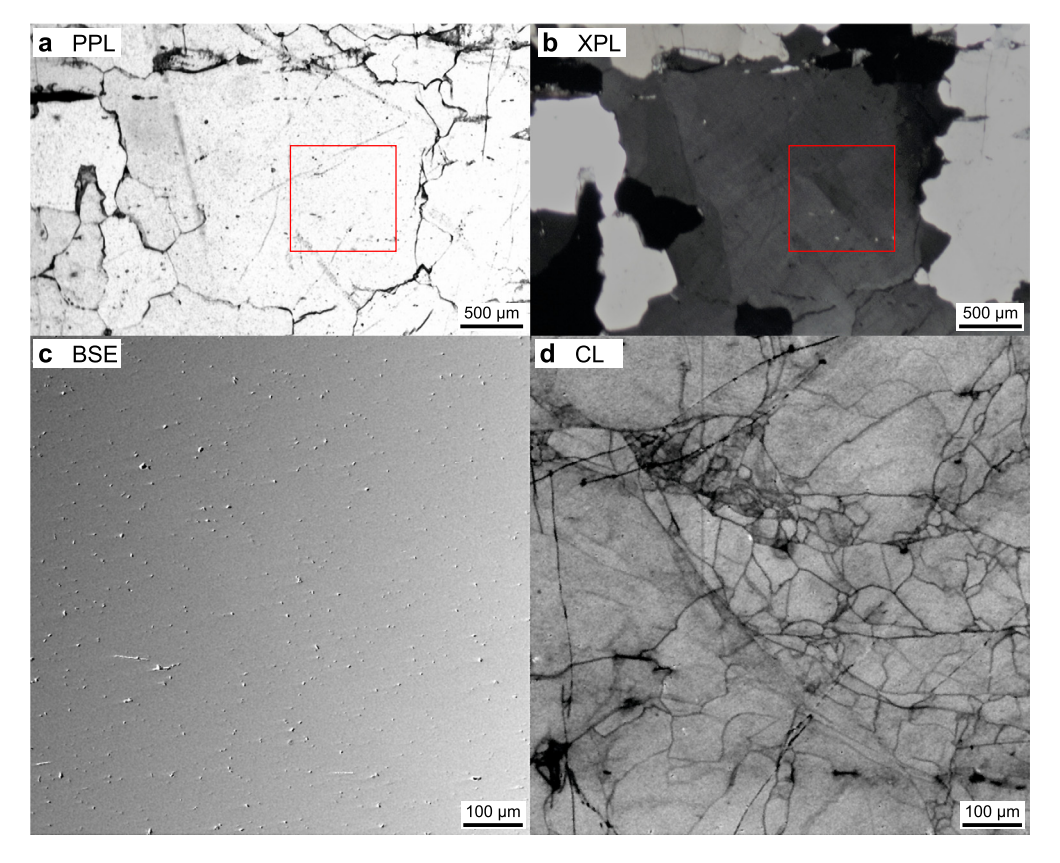


Fig. 8. Quartz grains from felsic granulite/amphibolite-facies rocks from the Grenville Orogen, Ontario, Canada. The field of view shows multiple quartz grains. (a) Plane-polarized light (PPL) photomicrograph. Note that the red box includes a small number of visible healed cracks that contain fluid inclusions. (b) Same area as (a) under cross-polarized light (XPL). Note that the red box contains what appears to be a subgrain with darker extinction. (c) Backscattered electron (BSE) image of area shown by red box in (a) and (b). Note the lack of evidence for surface topography that would typically occur if open cracks were present. (d) Cathodoluminescence (CL) image of area shown by red box in (a) and (b) showing many interconnected sinuous lines that are not visible in (a), (b) or (c). We interpret these as healed microcracks, and what appears to be undulose extinction in this and other quartz grains in the sample can be attributed to slight misorientations across these healed microcracks. The rock was metamorphosed in the granulite facies, and subsequently crossed into the amphibolite facies along a retrograde path similar to that shown in blue in Fig. 7 (Mills et al., 2017). We suggest that the healed microcracks may have formed during the $β \rightarrow α$ transition, and that the fragment boundary geometries were subsequently modified for example by smoothing of sharp corners at elevated temperature to reduce surface energy. (For interpretation of the colors in the figure, the reader is referred to the web version of this article.)

crossed the $\beta \to \alpha$ transition into the amphibolite-facies (Mills et al., 2017).

Considering the quartzo-feldspathic orthogneiss, sample MF223b (Fig. 1a) and crustal conditions corresponding to \sim 5, 10 and 18 km depth (-130, -270 and -480 MPa hydrostatic confining stress), Fig. 9 shows that hydrostatic loading would lead to 32.4%, 22.0% and 14.4%, respectively, of quadrature points exceeding the tensile strength threshold of 50 MPa when quartz undergoes the $\beta \rightarrow \alpha$ transition. If a tensile strength of 10 MPa is chosen (e.g., Mardon et al., 1990; You, 2015; Lan et al., 2019), 36.7%, 34.2% and 25.0% of quadrature points exceed the tensile strength threshold (Fig. 9). A nonhydrostatic macroscale stress field would increase those percentages accordingly, and there are compelling arguments for dry lower-crustal rocks sustaining large differential stresses (Jamtveit et al., 2016) that may further facilitate brittle damage. Although microcracks at these temperatures may heal rapidly in the presence of fluid, microcracking associated with the $\beta \rightarrow \alpha$ transition may initiate and accelerate metamorphic reactions by facilitating fluid access to reactants, and the positive volume changes associated with resulting hydration reactions would then continue the microcracking and fluid-access cycle. Grain size of quartz may be reduced near the $\alpha \leftrightarrow \beta$ transition through both brittle and viscous processes. In addition, hydration reactions generate heat and are therefore effective agents for strain localization. In the presence of enough differential stress, amphibolite-facies shear zones would form in the granulite-facies rocks in a feedback among transition-, strain- and hydration-induced weakening, and local seismicity may

also contribute to this feedback (Nikitin et al., 2009; Jamtveit et al., 2019).

Significant attention has recently been focused on the role of heterogeneous, grain-scale, elastic normal and mean stresses in metamorphic reactions (Tajčmanová et al., 2014; Hobbs and Ord, 2016; Jamtveit et al., 2016; Powell et al., 2018; Wheeler, 2018). In general, chemical equilibrium in dry or fluid-saturated deforming rocks is explicitly dependent on the grain-scale stresses (Dahlen, 1992), and the discussion centers around the degree of this dependence. Addressing this controversy, Figs. 6 and 9 show a large range of stresses at different hydrostatic confining pressures for β -quartz near the $\alpha \leftrightarrow \beta$ transition. Although some of the stress peaks in Figs. 6 and 9 may be reduced by brittle or viscous dissipation processes, their magnitudes would still span large ranges as governed by the elastic interactions of individual anisotropic grains.

6. Summary

We use natural rock microstructures combined with numerical experiments to investigate the grain-scale stresses that arise in quartz-bearing rocks loaded hydrostatically that pass either direction across the quartz $\alpha \leftrightarrow \beta$ phase transition. We find that the interactions of anisotropic grains in polyphase rocks during the down-temperature $\beta \rightarrow \alpha$ transition lead to large grain-scale tensile principal stresses and shear stresses that locally greatly exceed those sustainable by rocks and minerals in the continental

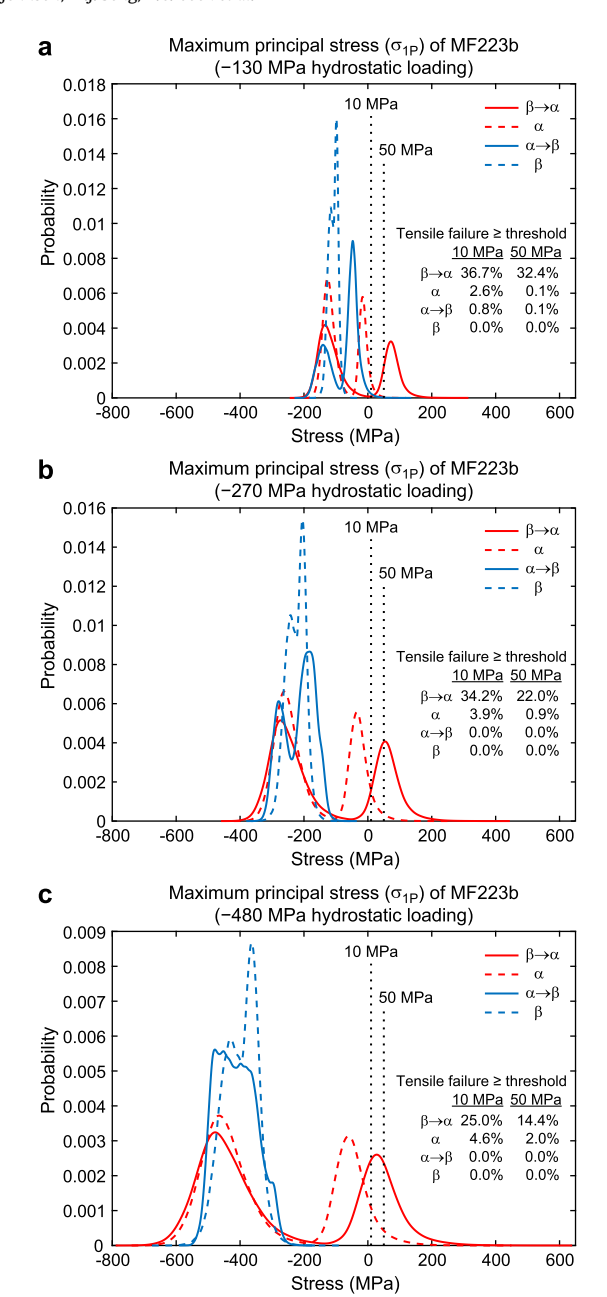


Fig. 9. Histograms showing the distributions of maximum principal stress for different confining pressures applied to quartzo-feldspathic orthogneiss (sample MF223b). (a) -130 MPa hydrostatic loading, (b) -270 MPa hydrostatic loading, (c) -480 MPa hydrostatic loading. The histograms are plotted for α -quartz just below the transition with no applied transition strains, β -quartz just above the transition with no applied transition strains, and the same α - and β -quartz with applied strains associated with the $\alpha \to \beta$ and $\beta \to \alpha$ transitions. The vertical dotted lines are two arbitrarily assumed tensile strengths of 10 and 50 MPa for reference. Tensile failure percentage is calculated by counting quadrature points above the tensile strength. All the histograms have the same x-axis scales to make comparisons. Note that with increasing confining pressure from (a) to (c), the ranges of the stress increase. (For interpretation of the colors in the figure, the reader is referred to the web version of this article.)

crust. Rapid increase in elastic strain energy would need to be dissipated by inelastic processes. If the phase transition for individual grains is effectively instantaneous, then quartz-bearing rocks crossing the $\beta \to \alpha$ transition may undergo inter- and intragranular microcracking in addition to viscous processes of stress dissipation. Since microcracking and surface energy generation is a relatively weak energy dissipation process, microcracking may be extensive before viscous processes can effectively contribute to reducing the

excess elastic strains. Because the grain-scale pressure leading up to the transition is heterogeneous in distribution and magnitude, favorably stressed and crystallographically oriented grains would begin to transition first, which would cause rapid local pressure changes and possibly trigger a cascade of transition over a finite Earth volume. If widespread microcracking occurs in response to the transition, transient permeability may facilitate the influx of fluids and initiate retrograde metamorphic reactions, which would then create a strong feedback owing to the volume increases associated with hydration reactions. Regardless of the mechanism of stress dissipation, brittle or viscous, the transition is likely to initiate or assist viscous strain localization.

CRediT authorship contribution statement

S.E.J. and W.J.S. designed and conducted the analysis. A.C.C., S.S.V. and C.C.G. contributed to analysis and presentation choices, and to the scientific interpretation of results. S.E.J. prepared the manuscript. W.J.S., A.C.C., S.S.V. and C.C.G. assisted in the writing. All authors contributed to development of the TESA numerical software, which was coded by A.C.C. in C and MATLAB.

Declaration of competing interest

The authors declare that they have no known competing financial interests or personal relationships that could have appeared to influence the work reported in this paper.

Acknowledgements

We acknowledge support from National Science Foundation grants EAR-0820946, EAR-1347087 and EAR-1727090. Maura Foley and Nancy Price collected samples MF223b and NAP57-08, respectively. Comments on an earlier version of this manuscript by Sandra Piazolo are gratefully acknowledged, as are constructive formal reviews by Andreas Kronenberg and Kevin Mahan.

Appendix A. Details of numerical methods to calculate grain-scale stresses

The purpose of our numerical analysis is to investigate changes in grain-scale stresses and strains arising from the $\alpha \leftrightarrow \beta$ phase transition in quartz under different macroscale loading conditions. To examine the relationships between the macroscale mechanical load, the microstructural response, and the resulting bulk properties, we require a multi-scale mathematical and computational approach. When a polycrystalline material is subjected to macroscale loads, the resulting microscale deformation can be decomposed into a homogeneous deformation (spatially uniform strains) plus displacement fluctuations due to microscale heterogeneities. The asymptotic expansion homogenization (AEH) method (Vel et al., 2016) relates the microscale displacement fluctuations to the macroscale strains and temperature change using 21 position-dependent proportionality constants known as characteristic functions. The characteristic functions explicitly account for the elastic interactions among individual grains. The 3-D elastic equilibrium equations at the microscale and Hooke's law for anisotropic materials yield a system of coupled partial differential equations for the 21 characteristic functions which are solved using the finite element (FE) method under periodic boundary conditions. Once computed, the characteristic functions enable the precise calculation of grain-scale field variables (Vel et al., 2016). Results from the AEH-FE method can vary markedly from those using averaging techniques such as the Voight, Reuss and Hill bounds, as demonstrated recently in calculating seismic wave velocities from

EBSD data (Naus-Thijssen et al., 2011; Vel et al., 2016; Almqvist and Mainprice, 2017; Cyprych et al., 2017).

To make the AEH-FE analysis convenient for users, we developed a stand-alone application called ThermoElastic and Seismic Analysis (TESA) Toolbox for Polycrystalline Materials (Vel et al., 2016; Cook et al., 2018), which features a MATLAB-based graphical user interface designed to analyze microstructures presented in a standard EBSD data-file format. The grain-scale stresses and strains are computed using the elastic properties of α - and β quartz (Ohno et al., 2006), plagioclase (Brown et al., 2016), alkali feldspar (Waeselmann et al., 2016), biotite (Aleksandrov and Ryzhova, 1961), and muscovite (Vaughan and Guggenheim, 1986). All calculations are fully three-dimensional, but EBSD data are twodimensional so the microstructure is extended into the third dimension. To reach convergence in the calculation of grain-scale field variables, the finite element mesh density needs to exceed \sim 60-100 elements/grain (Vel et al., 2016). The ratio of elements to grains exceeds 100 in all our models (Table S1). Similarly, the number of grains should be large enough to be representative of the microstructure. Young's modulus in polycrystalline zinc with \sim 200 grains differ by only \sim 4% from results with several thousand grains (Vel et al., 2016). The number of grains in our models ranges from 219 to 1327 (Table S1).

All quartz grains in the homogeneous transition case simultaneously undergo an expansion or contraction. In addition, for the purposes of our study, we assume that all minerals are perfectly bonded together with traction and displacement continuity across the grain-boundaries. Our results for the homogeneous transition case (Figs. 2 and S4) therefore generally yield maximum local and model-scale stresses associated with the transition.

Accumulation of large, essentially instantaneous elastic stresses in nature would activate inelastic processes such as microcracking, which would lead to progressive changes in the magnitudes and distributions of local stresses and strains. The computational modeling of multiple crack propagation in brittle polycrystalline materials is challenging due to the difficulties associated with the calculation of stress intensity factors at each crack tip. Thus, for the heterogeneous transition case (Figs. 4 and 5; Animations S1 and S2), we utilize a micromechanical damage model (e.g., Ren et al., 2011) for the accurate characterization of microscale damage. Microscale damage is governed by the maximum stress criterion. If σ_{1P} of an element exceeds the assigned tensile strength, its elastic compliance in the direction of σ_{1P} is increased by 10% to simulate the reduction of stiffness associated with brittle damage under moderate confining pressure. As the triangular finite elements become damaged, a line is drawn through their interiors connecting neighboring damaged elements. As the damage analysis proceeds, all elements are free to damage along multiple planes depending on the damage state of neighboring elements.

Appendix B. Supplementary material

Supplementary material related to this article can be found online at https://doi.org/10.1016/j.epsl.2020.116622.

References

- Abers, G.A., Hacker, B.R., 2017. A MATLAB toolbox and Excel workbook for calculating the densities, seismic wave speeds, and major element composition of minerals and rocks at pressure and temperature. Geochem. Geophys. Geosyst. 17, 616–624. https://doi.org/10.1002/2015GC006171.
- Aleksandrov, K.S., Ryzhova, T.V., 1961. Elastic properties of rock-forming minerals, II: layered silicates. Bull. Acad. Sci. USSR, Geophys. Ser. (Engl. Transl.) 12, 1165–1168.
- Almqvist, B.S.G., Mainprice, D., 2017. Seismic properties and anisotropy of the continental crust: predictions based on mineral texture and rock microstructure. Rev. Geophys. 55, 367–433. https://doi.org/10.1002/2016RG000552.

- Blereau, E., Johnson, T.E., Clark, C., Taylor, R.J.M., Kinny, P.D., Hand, M., 2017. Reappraising the P–T evolution of the Rogaland–Vest Agder Sector, southwestern Norway. Geosci. Front. 8, 1–14. https://doi.org/10.1016/j.gsf.2016.07.003.
- Brown, M., 2007. Metamorphic conditions in orogenic belts: a record of secular change. Int. Geol. Rev. 49, 193–234. https://doi.org/10.2747/0020-6814.49.3.193.
- Brown, J.M., Angel, R.J., Ross, N.L., 2016. Elasticity of plagioclase feldspars. J. Geophys. Res. 121, 663–675. https://doi.org/10.1002/2015JB012736.
- Carpenter, M.A., Salje, E.K.H., Graeme-Barber, A., Wruck, B., Dove, M.T., Knight, K.S., 1998. Calibration of excess thermodynamic properties and elastic constant variations associated with the alpha <-> beta phase transition in quartz. Am. Mineral. 83, 2–22. https://doi.org/10.2138/am-1998-1-201.
- Coe, R.S., Paterson, M.S., 1969. The α - β inversion in quartz: a coherent phase transition under nonhydrostatic stress. J. Geophys. Res. 74, 4921–4948. https://doi.org/10.1029/J8074i020p04921.
- Cook, A.C., Vel, S.S., Johnson, S.E., Gerbi, C.C., Song, W.J., 2018. ThermoElastic and seismic analysis (TESA) toolbox for polycrystalline materials. https://umaine. edu/mecheng/vel/software/tesa_toolbox/.
- Cyprych, D., Piazolo, S., Almqvist, B.S.G., 2017. Seismic anisotropy from compositional banding in granulites from the deep magmatic arc of Fiordland, New Zealand. Earth Planet. Sci. Lett. 477, 156–167. https://doi.org/10.1016/j.epsl.2017. 08.017.
- Dahlen, F.A., 1992. Metamorphism of nonhydrostatically stressed rocks. Am. J. Sci. 292, 184–198. https://doi.org/10.2475/ajs.292.3.184.
- Doncieux, A., Stagnol, D., Huger, M., Chotard, T., Gault, C., Ota, T., Hashimoto, S., 2008. Thermo-elastic behaviour of a natural quartzite: itacolumite. J. Mater. Sci. 43, 4167–4174. https://doi.org/10.1007/s10853-007-2414-z.
- Ghiorso, M.S., Carmicheal, I.S.E., Moret, L.K., 1979. Inverted high-temperature quartz. Contrib. Mineral. Petrol. 68, 307–323. https://doi.org/10.1007/BF00371553.
- Glover, P.W.J., Baud, P., Darot, M., Meredith, P.G., Boon, S.A., LeRavalec, M., Zoussi, S., Reuschlé, T., 1995. α/β phase transition in quartz monitored using acoustic emissions. Geophys. J. Int. 120, 775–782. https://doi.org/10.1111/j.1365-246X. 1995.tb01852.x.
- Hobbs, B.E., Ord, A., 2016. Does non-hydrostatic stress influence the equilibrium of metamorphic reactions? Earth-Sci. Rev. 163, 190–233. https://doi.org/10.1016/j. earscirev.2016.08.013.
- Jamtveit, B., Austrheim, H., Putnis, A., 2016. Disequilibrium metamorphism of stressed lithosphere. Earth-Sci. Rev. 154, 1–13. https://doi.org/10.1016/j. earscirev.2015.12.002.
- Jamtveit, B., Petley-Ragan, A., Incel, S., Dunkel, K.G., Aupart, C., Austrheim, H., Corfu, F., Menegon, L., Renard, F., 2019. The effects of earthquakes and fluids on the metamorphism of the lower continental crust. J. Geophys. Res. 124, 7725–7755. https://doi.org/10.1029/2018JB016461.
- Kern, H., 1979. Effect of high-low quartz transition on compressional and shear wave velocities in rocks under high pressure. Phys. Chem. Miner. 4, 161–171. https://doi.org/10.1007/bf00307560.
- Kuo-Chen, H., Wu, F.T., Jenkins, D.M., Mechie, J., Roecker, S.W., Wang, C.-Y., Huang, B.-S., 2012. Seismic evidence for the α - β quartz transition beneath Taiwan from Vp/Vs tomography. Geophys. Res. Lett. 39, L22302. https://doi.org/10.1029/2012C1053649
- Lakshtanov, D.L., Sinogeikin, S.V., Bass, J.D., 2007. High-temperature phase transitions and elasticity of silica polymorphs. Phys. Chem. Miner. 34, 11–22. https://doi.org/10.1007/s00269-006-0113-y.
- Lan, H., Chen, J., Macciotta, R., 2019. Universal confined tensile strength of intact rock. Sci. Rep. 9, 6170. https://doi.org/10.1038/s41598-019-42698-6.
- Lawn, B., Marshall, D., Raj, R., Hirth, G., Page, T., Yeomans, J., 2020. Precipitous weakening of quartz at the α - β phase inversion. J. Am. Ceram. Soc. https://doi.org/10.1111/jace.17470.
- Mardon, D., Kronenberg, A.K., Handin, J., Friedman, M., Russell, J.E., 1990. Mechanisms of fracture propagation in experimentally extended Sioux quartzite. Tectonophysics 182, 259–278. https://doi.org/10.1016/0040-1951(90)90167-7.
- Marini, L., Manzella, A., 2005. Possible seismic signature of the α – β quartz transition in the lithosphere of Southern Tuscany (Italy). J. Volcanol. Geotherm. Res. 148, 81–97. https://doi.org/10.1016/j.jvolgeores.2005.03.015.
- Mechie, J., Sobolev, S.V., Ratschbacher, L., Babeyko, A.Y., Bock, G., Jones, A.G., Nelson, K.D., Solon, K.D., Brown, L.D., Zhao, W., 2004. Precise temperature estimation in the Tibetan crust from seismic detection of the α - β quartz transition. Geology 32, 601–604. https://doi.org/10.1130/G20367.1.
- Mills, S.G., Gerbi, C., Marsh, J.H., Yates, M.G., Seaman, S.J., White, J.C., 2017. Tectonic and chemical implications of cathodoluminescent microstructures in quartz, Parry Sound domain, Ontario, Canada. Can. J. Earth Sci. 54, 677–692. https:// doi.org/10.1139/cjes-2016-0168.
- Naus-Thijssen, F.M.J., Goupee, A.J., Vel, S.S., Johnson, S.E., 2011. The influence of microstructure on seismic wave speed anisotropy in the crust: computational analysis of quartz-muscovite rocks. Geophys. J. Int. 185, 609–621. https://doi. org/10.1111/j.1365-246X.2011.04978.x.
- Nikitin, A.N., Vasin, R.N., Balagurov, A.M., Sobolev, G.A., Ponomarev, A.V., 2006. Investigation of thermal and deformation properties of quartzite in a temperature range of polymorphous α - β transition by neutron diffraction and acoustic emission methods. Phys. Part. Nucl. Lett. 3, 46–53. https://doi.org/10.1134/S1547477106010067.

- Nikitin, A.N., Vasin, R.N., Rodkin, M.V., 2009. Possible influence of polymorphic transitions in minerals (according to the quartz example) on seismotectonic processes in the lithosphere. Izv. Phys. Solid Earth 45, 338–346. https://doi.org/10.1134/S1069351309040065.
- Ohno, I., Harada, K., Yoshitomi, C., 2006. Temperature variation of elastic constants of quartz across the α β transition. Phys. Chem. Miner. 33, 1–9. https://doi.org/10.1007/s00269-005-0008-3.
- Peng, Z., Redfern, S.A.T., 2013. Mechanical properties of quartz at the α - β phase transition: implications for tectonic and seismic anomalies. Geochem. Geophys. Geosyst. 14, 18–28. https://doi.org/10.1029/2012GC004482.
- Powell, R., Evans, K.A., Green, E.C.R., White, R.W., 2018. On equilibrium in non-hydrostatic metamorphic systems. J. Metamorph. Geol. 36, 419–438. https://doi.org/10.1111/jmg.12298.
- Ren, X., Chen, J.-S., Li, J., Slawson, T.R., Roth, M.J., 2011. Micro-cracks informed damage models for brittle solids. Int. J. Solids Struct. 48, 1560–1571. https:// doi.org/10.1016/j.ijsolstr.2011.02.001.
- Richter, B., Stünitz, H., Heilbronner, R., 2016. Stresses and pressures at the quartz-to-coesite phase transformation in shear deformation experiments. J. Geophys. Res. 121, 8015–8033. https://doi.org/10.1002/2016JB013084.
- Schmidt, C., Bruhn, D., Wirth, R., 2003. Experimental evidence of transformation plasticity in silicates: minimum of creep strength in quartz. Earth Planet. Sci. Lett. 205, 273–280. https://doi.org/10.1016/S0012-821X(02)01046-4.
- Sharon, E., Gross, S.P., Fineberg, J., 1996. Energy dissipation in dynamic fracture. Phys. Rev. Lett. 76, 2117–2120. https://doi.org/10.1103/PhysRevLett.76.2117.
- Sheehan, A.F., de la Torre, T.L., Monsalve, G., Abers, G.A., Hacker, B.R., 2014. Physical state of Himalayan crust and uppermost mantle: constraints from seismic attenuation and velocity tomography. J. Geophys. Res. 119, 567–580. https://doi.org/10.1002/2013|B010601.
- Shen, A.H., Bassett, W.A., Chou, I.-M., 1993. The α - β quartz transition at high temperatures and pressures in a diamond-anvil cell by laser interferometry. Am. Mineral, 78, 694–698.
- Spear, F.S., 1992. Thermobarometry and P-T paths from granulite facies rocks: an introduction. Precambrian Res. 55, 201–207. https://doi.org/10.1016/0301-9268(92)90024-I.
- Tajčmanová, L., Podladchikov, Y., Powell, R., Moulas, E., Vrijmoed, J.C., Connolly, J.A.D., 2014. Grain-scale pressure variations and chemical equilibrium in high-grade

- metamorphic rocks. J. Metamorph. Geol. 32, 195–207. https://doi.org/10.1111/img.12066.
- Van der Molen, I., 1981. The shift of the α - β transition temperature of quartz associated with the thermal expansion of granite at high pressure. Tectonophysics 73, 323–342. https://doi.org/10.1016/0040-1951(81)90221-3.
- Vaughan, M.T., Guggenheim, S., 1986. Elasticity of muscovite and its relationship to crystal structure. J. Geophys. Res. 91, 4657–4664. https://doi.org/10.1029/ JB091iB05p04657.
- Vel, S.S., Cook, A.C., Johnson, S.E., Gerbi, C., 2016. Computational homogenization and micromechanical analysis of textured polycrystalline materials. Comput. Methods Appl. Math. 310, 749–779. https://doi.org/10.1016/j.cma.2016.07.037.
- Vernon, R.H., Clarke, G.L., 2008. Principles of Metamorphic Petrology. Cambridge University Press, United Kingdom.
- Waeselmann, N., Brown, J.M., Angel, R.J., Ross, N., Zhao, J., Kaminsky, W., 2016. The elastic tensor of monoclinic alkali feldspars. Am. Mineral. 101, 1228–1231. https://doi.org/10.2138/am-2016-5583.
- Wenk, H.-R., Barton, N., Bertolotti, M., Vogel, S.C., Voltolini, M., Lloyd, G.E., Gonzalez, G.B., 2009. Dauphiné twinning and texture memory in polycrystalline quartz. Part 3: texture memory during phase transformation. Phys. Chem. Miner. 36, 567–583. https://doi.org/10.1007/s00269-009-0302-6.
- Wheeler, J., 2018. The effects of stress on reactions in the Earth: sometimes rather mean, usually normal, always important. J. Metamorph. Geol. 36, 439–461. https://doi.org/10.1111/jmg.12299.
- You, M., 2015. Strength criterion for rocks under compressive-tensile stresses and its application. J. Rock Mech. Geotech. Eng. 7, 434–439. https://doi.org/10.1016/ j.jrmge.2015.05.002.
- Zappone, A.S., Benson, P.M., 2013. Effect of phase transitions on seismic properties of metapelites: a new high-temperature laboratory calibration. Geology 41, 463–466. https://doi.org/10.1130/G33713.1.
- Zhang, Z., Xiang, H., Dong, X., Ding, H., He, Z., 2015. Long-lived high-temperature granulite-facies metamorphism in the Eastern Himalayan orogen, south Tibet. Lithos 212–215, 1–15. https://doi.org/10.1016/j.lithos.2014.10.009.